PCCP

PAPER

Cite this: *Phys. Chem. Chem. Phys.*, 2017, **19**, 32125

Crystal phase transition of urea: what governs the reaction kinetics in molecular crystal phase transitions†

Cheng Shang, * Xiao-Jie Zhang and Zhi-Pan Liu *

Received 17th October 2017,
Accepted 20th November 2017

DOI: 10.1039/c7cp07060h

rsc.li/pccp

Because of their weak intermolecular forces and flexible molecular geometry, molecular crystals are renowned for their structural versatility (polymorphism) and the great difficulty in controlling the crystal form during synthesis. Despite its great importance in determining the final solid form (*e.g.* single crystal, polycrystal or amorphous), the kinetics of the crystal-to-crystal transformation between structures with different molecular packing has long been a fundamental challenge in both measurement and simulation. Here we report the first global potential energy surface (PES) for urea crystals obtained by stochastic surface walking global PES exploration. With the big data from thousands of crystal/amorphous forms, we, using exhaustive reaction pathway sampling, resolve the solid-to-solid transformation pathways between urea crystals from first principles. We demonstrate that the strong tendency to grow a large single crystal of urea can be attributed to the flat PES between major crystal forms that share the same hydrogen-bonding network pattern, where one crystal can transform to another facilely *via* crystal-to-crystal transition. Other crystal forms with distinct hydrogen-bonding network patterns can be excluded in crystallization due to their poor thermodynamic stability and high barrier of solid-to-solid transition. A general theory for predicting molecular solid transformation is proposed and illustrated in a simplified one-dimensional global PES, which is now obtainable from computational techniques established here.

1. Introduction

Recent years have seen tremendous progress in the applications of molecular crystals, ranging from pharmaceutical applications to OLED devices.[1–4] The molecular crystal properties depend sensitively on the crystal structure and thus the kinetics of crystal-to-crystal solid phase transition is of key importance in applications. For example, a fast crystal phase transition can be exploited to transform chemical energy into mechanical energy,[5] whereas a high stability of molecular crystal structures is highly desirable in drug delivery.[6] Considering that the weak van der Waals (vdW) interaction is believed to dominate the molecular packing, how to promote or slow the crystal-to-crystal transition remains a great challenge in molecular crystal synthesis and engineering. Urea, as a textbook example of a molecular crystal, was firstly synthesized by Friedrich Wöhler in 1828, and has triggered the development of organic chemistry. While urea is known to crystalize rapidly in solution, recent studies suggest that a crystal-to-crystal phase transition occurs in the crystallization process, mediating the fast growth of a large urea crystal.[7,8] Due to the difficulty in characterizing the nascent crystal nuclei, both from experiment and from theory, little knowledge is available to date to understand the kinetics of molecular crystal phase transition and its roles in crystallization.

While there are many likely low energy crystal forms for a molecular crystal in general, limited crystal forms can be confirmed in either experiment or theory. Experimentally, three crystal structures of urea, *i.e.* phase **I** (ambient phase), phase **III**, and phase **IV** (high pressure phases) have been characterized in the literature[9] and the obtained phase diagram suggests subtle energy differences between them, *i.e.* within $\sim$1.3 kcal mol^{-1}. Among the three major N–H$\cdots$O hydrogen-bonding (H-bonding) patterns between urea molecules (see Fig. 1), only type-I and type-II are present in the known crystal phases and it is unclear why type-III is only observed in urea-containing co-crystals,[9] where urea is utilized as a reagent to facilitate crystallization of other molecules. Theoretically, using metadynamics and the

Collaborative Innovation Center of Chemistry for Energy Material, Shanghai Key Laboratory of Molecular Catalysis and Innovative Materials, Key Laboratory of Computational Physical Science (Ministry of Education), Department of Chemistry, Fudan University, Shanghai 200433, China. E-mail: cshang@fudan.edu.cn, zpliu@fudan.edu.cn

† Electronic supplementary information (ESI) available: The structure information of other crystal structures for urea; pathway for the transformation from crystal **B** to **C**; XYZ coordinates for key crystals; movies showing transformation pathways from phase **IV** to **I** and phase **IV** to **III**. See DOI: 10.1039/c7cp07060h

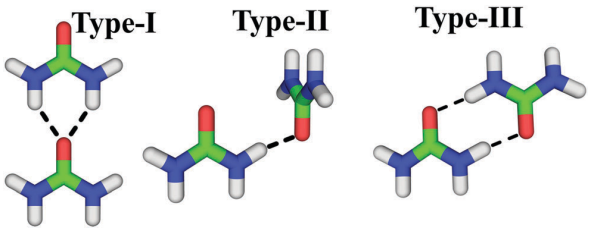

Fig. 1 Main H-bonding motif (or supramolecular synthons[2]) observed in urea-containing molecular crystals.

generalized amber force field (GAFF),[7] Giberti *et al.* discovered a new crystal form that can exist below 420 K, being 10 kJ mol^{-1} less stable than phase **I** using DFT calculations. The new phase was then named as form II that is composed of cyclic dimers with a type-III hydrogen bond (H-bond). The form II to phase **I** transition, a crystal-to-crystal transformation reaction, was observed in simulation at 420 K with 300 urea molecules in the simulation box. Similarly, Mandal and Larson have observed reverse crystal-to-crystal transformation during the dissolving of urea clusters using long-time unbiased molecular dynamics (MD) simulations.[8] These results suggest that the crystal form II and its transition to phase **I** contributes greatly to the rapid crystallization of urea. To add more complexity, the identified crystal forms in theoretical simulation, such as the form II in urea, may in fact be transient and difficult to observe in experiments despite their great importance in the kinetics during crystal nucleation. Apparently, a large gap is present in our knowledge base on the transformation between different crystal forms of a molecular crystal, which are difficult to obtain from current techniques, both experimental and theoretical.

Here we take the textbook example, urea crystals, to investigate the kinetics of the crystal-to-crystal phase transition. By using stochastic surface walking (SSW) global optimization,[10,11] we establish for the first time the global potential energy surface (PES) of urea. Unlike the conventional structure prediction where the most stable crystal form (global minimum, GM) is targeted, here we look for those metastable, less ordered crystal forms that are transient but critical to the crystal transition kinetics. From the DFT (BEEF-vdW)[12] calculations, we identify 11 urea crystal structures that are close in energy to the GM, including the observed ones in the experiments and theoretical simulations. By searching for low energy pathways between all these crystal forms, we resolve the physical origin of the rapid crystal-to-crystal phase transition in urea. We show that the dominant type-I H-bonding network in urea leads to fast solid-to-solid transformations among metastable phases. The tools and the theory established can be applied in general to study the crystal transformation in molecular crystals.

2. Calculation methods

2.1. Reaction pathway sampling based on the SSW method

In this work, the SSW method is first utilized to explore the PES of the urea crystals. The SSW method is capable of surmounting the high barrier on the PES and identifying low energy minima and at the same time collects the reaction pathways leading to them.[10,11] The efficiency of the method for exploring PESs has been demonstrated in many crystals.[13] SSW based reaction sampling (SSW-RS)[14] is then utilized to sample the solid reaction pathways, exhaustively and unbiasedly, from which we obtain the crystal-to-crystal solid phase transition pathway between interesting minima. For solid phase transitions, this is to identify the one-to-one correspondence for the lattice (L (e_1, e_2, e_3), e_i being the lattice vector) and atom (q_i, i = 1,…, 3N, N is the number of atoms in the cell) from one crystal phase (the initial state, IS) to another (the final state, FS), which constitutes the reaction coordinates of the reaction, *i.e.*, Q_{IS} (L, q) → Q_{FS} (L, q). In one SSW pathway sampling simulation, we need to collect as many IS/FS pairs as possible (typically a few hundreds) to ensure the identification of the best reaction coordinate, the one corresponding to the lowest energy pathway. With such a pair of reaction coordinates, Q_{IS} (L, q) and Q_{FS} (L, q), it is then possible to utilize the variable-cell double-ended surface walking (VC-DESW) method to identify the reaction transition state (TS) and the minimum energy pathway. In our implementation, the SSW pathway sampling is fully automated and divided into three stages in the simulation, namely, (i) pathway collection *via* extensive SSW global search; (ii) pathway screening *via* fast DESW pathway building; and (iii) lowest energy pathway determination *via* DESW TS search. The first stage is the most important and most time-consuming part, which generates all the likely pairs of generalized reaction coordinates linking different crystal phases. More details on the SSW method and SSW pathway sampling are described in our previous studies.[10,11,15,16] For urea crystal-to-crystal transition, we have utilized SSW sampling to collect the likely pathways between all low energy crystal forms. More than 2 × 10^4 SSW runs are performed for each crystal phase using the Amber force field. All the distinct pathways are screened using DESW methods and the ones with low barriers are refined using DFT calculations.

2.2. Force field and DFT details

The potential energy surface exploration was performed with the amber force field implemented in LAMMPS.[15] The amber ff99SB molecular mechanics force field[16] was utilized to evaluate the potential energy and the derivatives. The partial charges used to generate the amber force field were calculated using GAMESS[17] at the B3LYP/6-31G* level[18–20] with the restricted electrostatic potential method.[21] The other force field parameters were taken from the general amber force field (gaff) parameter set.[22] This type of force field has been utilized to simulate urea crystallization in many studies.[7,8,23,24]

The DFT calculations were performed using the plane wave DFT program, Vienna ab initio simulation package VASP,[25,26] where electron–ion interaction was represented by the projector augmented wave (PAW) pseudopotential[27] and the exchange–correlation functional utilized was the Bayesian error estimation functional with vdW correlation (BEEF-vdW).[12] A plane wave basis set cutoff energy of 600 eV was used, and Brillouin zone integrations were performed on a Monkhorst–Pack grid with a

k-point spacing of approximately 0.05 Å^{-1}. The convergence for the electronic structure calculations is set to be less than 2×10^{-6} eV energy change between consecutive iteration steps. All the structures are optimized using a Quasi-Newton BFGS method until the maximal force component on the atoms is below 0.001 eV Å^{-1} and the stress is below 0.001 GPa. For all the low energy minima reported in this work, their geometry including the lattice parameters and the atomic position are converged successfully in both Amber force field and DFT calculations. No symmetry constraint is used in the geometry optimization or SSW global optimization.

3. Results and discussion

We first utilize the standard Amber ff99SB molecular mechanics force field[16] in combination with the SSW method to exhaustively explore the configuration space and to identify the reaction pathways between key minimum structures, including the major crystal forms and amorphous forms. The Amber ff99SB method has been shown to reproduce accurately the lattice parameters and melting temperature of urea and also a number of organic molecules.[23,24] For the close energetics between molecular crystals, we then utilize first principles density functional theory (DFT) calculations with the Bayesian error estimation functional with vdW correlation (BEEF-vdW)[12] to refine the structure and energetics for the major minima and all low energy solid-to-solid phase transition pathways. It should be emphasized that all the energetic data reported in this work, including the reaction barriers, unless explicitly mentioned, are computed from DFT (BEEF-vdW).

Our SSW simulations were carried out massively in parallel by using a series of supercells up to 8-molecules per cell starting from random molecular packing. In total, 10^5 minimum structures are visited and 4526 distinct minima for urea are identified from SSW trajectories, which constitutes the global PES of urea. With these data, we are able to examine the classic Kitaigorodskii rule:[28] the linear relationship between energy (E) and the volume (Vol) of the structure, which should provide a first overview on the complexity of the global PES. As shown in Fig. 2a, we plot the E against Vol from the SSW minima (Amber force field) for urea, which are compared with those from two other molecules, acrolein and ethane (molecules with a similar size to urea examined for the purpose of comparison). We found that the Vol–E correlation is largely linear in all cases, confirming that the Kitaigorodskii rule is valid in a large energy scale. The urea deviates more obviously from this rule with the poorest linearity (R^2 = 0.90). This suggests that the global PES of urea is more complex and the interaction between urea molecules is not governed purely by the isotropic vdW forces. Indeed, from the molecular structure, one would expect that strong H-bond networks are present for urea, while ethane has only vdW intermolecular interaction (R^2 = 0.99) and acrolein, despite being polarized, lacks strong H-bonds (R^2 = 0.95). This may explain why the GM of urea is not the densest form, while it is for both ethane and acrolein.

Since the dense packing is not the only driving force that leads to the lowest energy crystal form, it is necessary to identify other structure descriptors to better distinguish different crystal forms and thus to establish the structure-energy correlation. Inspired by the large dipole moment of urea (4.56 D) compared to that of acrolein (3.11 D) and ethane (0 D), we have designed a distance-weighted Steinhardt-type order parameter,[29,30] OP$_l$ (degree l = 4, which gives the best distinction between minima) as defined in eqn (1) and (2) to measure the dipole arrangement pattern nearby a molecule in the crystal. The contribution of dipole vectors $\vec{\mathbf{v}}$ of nearby molecules is summed *via* a spherical function, as weighted by the distance between molecules.

$$\mathrm{OP}_l = \frac{\sum_{j=1}^{\mathrm{nmol}} \sqrt{\frac{4\pi}{2l+1} \sum_{m=-l}^{l} \left| \sum_{i}^{r_{ij} < r_{\max}} \lambda_{ij} \cdot Y_{lm}(\vec{\mathbf{v}}_i) \right|^2}}{\sum_{ij} \lambda_{ij}} \quad (1)$$

$$\lambda_{ij} = \exp\left(-\frac{1}{2} \times \max\left(0, \frac{r_{ij} - r_0}{r_0} \right) \right) \quad (2)$$

In eqn (1) and (2), nmol is the number of molecules in the unit cell, which is no greater than 8 in this work; Y_{lm} is the spherical harmonic function of degree l and order m; λ_{ij} is the distance-weighting factor; r_{ij} is the intermolecular distance between the center of mass of molecule i and j; r_0 is a typical shortest intermolecular distance between neighbouring molecules, being set as 4 Å; $\vec{\mathbf{v}}_i$ is the dipole vector of molecule "i"; the index i runs for all molecules surrounding molecule j (including j itself) in the supercell with a distance r_{ij} smaller than $r_{\max}$, which is $r_{\max}$ = 15 Å in this work. By this definition, OP$_4$ = 1 if all the dipoles align in parallel in the crystal; and OP$_4$ would be close to zero if the dipoles distributed randomly.

We then plotted in Fig. 2b for all minima the energy against this geometry fingerprint OP$_4$ to visualize the global PES of urea. The density of state (DOS) is the Boltzmann-weighted DOS as obtained from the SSW trajectory. From the E–OP global PES plot, one can readily distinguish crystal structures from amorphous ones, which are separated roughly at 1.5 kcal mol^{-1} above the GM (dotted black line in Fig. 2b). Above it, the PES enters into the amorphous region, which has a high and continuous DOS, containing numerous energy-degenerate structures (deep blue colour in DOS); the center of the amorphous region has an OP$_4$ value of 0.4, indicating poor alignment for the dipoles of molecules in the cell. Below it is the crystalline region, where 25 distinct minima within 1 kcal mol^{-1} from the GM are identified using Amber and refined using DFT. Seven new crystal structures in total are found to be within 1 kcal mol^{-1} from the GM after DFT refinement (shown in ESI,† Fig. S1). From 25 minima, we labelled six representative minima (phase **I**, **III**, **IV**, **A**, **B**, **C**) on the PES in Fig. 2b and listed their properties in Table 1. The crystal **A** is the previously identified form II from simulation. Most minima in the crystalline region have OP$_4$ values larger than 0.5, indicating a much better dipole alignment between molecules compared to the amorphous structures. In particular, for three experimental observed phases, the OP$_4$ values

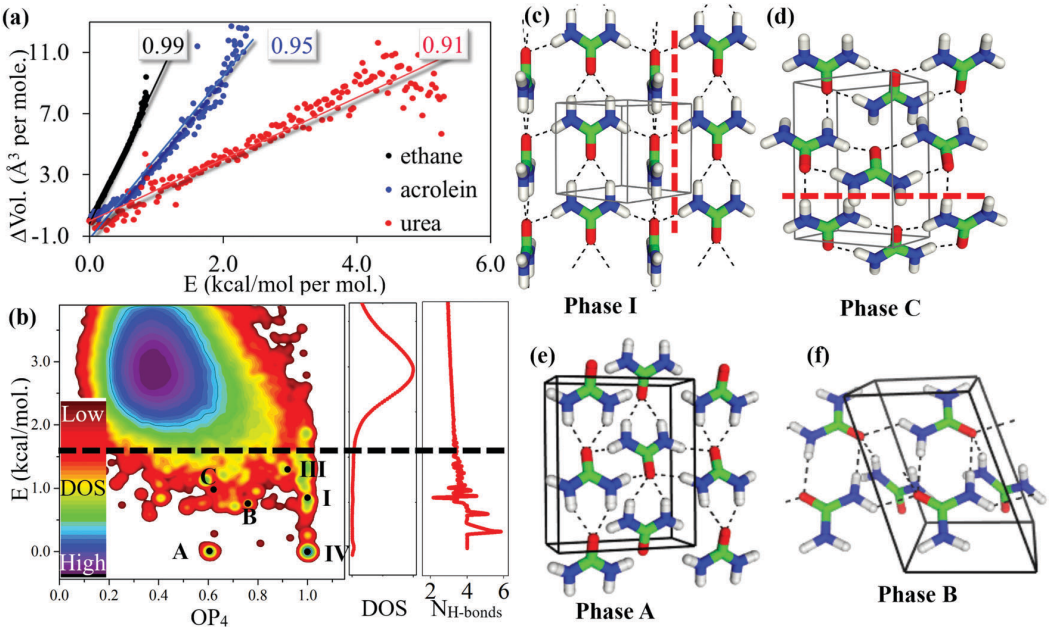

Fig. 2 SSW global PES exploration of urea using Amber force-field. (a) Volume–energy plots for all minima of urea (red), acrolein (blue) and ethane (black) with the correlation coefficient of linear fitting being 0.91, 0.95 and 0.99, respectively. (b) Two-dimensional global PES of urea minima from SSW trajectories projected onto energy (*y*-axis, with reference to the GM) and structure fingerprints as described by the Steinhardt type order parameter (*x*-axis, eqn (1)). **I** to **III** and **A** to **C** label important crystalline structures that are listed in Table 1. The density of states (DOS) and the average number of hydrogen bonds ($N_{\text{H-bonds}}$) are also shown; (c–f) the atomic structures for crystal **I** and **A** to **C** (labelled in (a)).

Table 1 Six representative crystal structures of urea[a]

Phase	S.G.	Vol.	$N_{\text{H-bond}}$[b]	$L_{\text{H-bond}}$	E	E_a
IV	$P2_12_12$	76.3	4(I + II)	2.16(I), 2.11(II)	0.0	0.06
A	*Pnma*	75.9	4(I + III)	2.20(I), 2.14(III)	0.95	0.18
B	$P\bar{1}$	74.0	3(III)	1.99(III)	0.54	2.24
I	$P\bar{4}2_1m$	78.4	4(I + II)	2.14(I), 2.09(II)	−0.04	0.07
C	$P2_1/b$	79.1	3(I + III)	2.06(I), 1.99(III)	0.87	0.40
III	$P2_12_12_1$	75.1	3(I + II)	2.16(I), 1.96(II)	−0.30	—

[a] Listed data are all from DFT (BEEF-vdW) calculations, including the symmetry group (S.G.), the volume (Å^3 mol^{-1}), the average number of H-bonds per molecule ($N_{\text{H-bond}}$), the average bond length of the H-bonds ($L_{\text{H-bond}}$, Å), the relative energy (E) with reference to phase **IV**, and the reaction barrier (E_a) to phase **III**. All energies are in the units of kcal mol^{-1}. [b] I, II and III describe the H-bond network pattern in Fig. 1.

are all equal or close to 1.0. For crystals **A** and **C**, the OP_4 values are 0.6, right below the amorphous region, suggesting that those minima are less ordered in the short-range and configurationally closer to the amorphous structures. We also carried out similar SSW PES exploration in a larger unit cell containing 16 molecules. The PES in the large-cell is now shown in Fig. S3 in the ESI.† We did not find any better crystal forms in the large-cell simulation. We emphasize that, while there are much more amorphous structures in the PES of large-cell simulation (as expected from the larger degree of freedoms), the main features of the PES as comparing Fig. 2b (8-molecule cell) and Fig. S3 (ESI†) (16-molecule cell) are in fact similar. The crystal–amorphous boundary appears roughly at 1.5 kcal mol^{-1} above the GM. There are many crystal forms with OP_4 = 1.0, suggesting that the type-I H-bond network dominates the low energy crystal forms.

By inspecting all 25 crystal structures together with phase **III**, we found that all three types of H-bond (Fig. 1) network are present for urea crystals. The network with type-I H-bonds is the most common, thus this is the principal H-bond motif, appearing in 18 structures. Among them, 11 crystals also contain the type-II pattern to form a 3-D linkage, including all three experimentally observed phases **IV** (the GM), **I** and **III**. Networks with type-III H-bonds are less popular, found only in 7 crystals, including **A**, **B** and **C**. In Fig. 2c–f, we highlight the structures of crystals **A**–**C**. Phase **I** can be regarded as a type-I H-bond skeleton with mutually orthogonal chains (along the red dashed line in Fig. 2c) cross-linked by a type-II H-bond network. Such a structure guarantees the parallel arrangement of all the dipoles in the crystal, which is also presented in other crystal forms with OP_4 = 1.0, such as phase **IV**. The crystal **C** (also **A** and **B**) is constituted by type-III chains (along the red dashed line in Fig. 2d), where the chain–chain interaction belongs to incomplete type-I H-bonds (circled dimer in Fig. 2d). It is noticed that the average number of H-bonds ($N_{\text{H-bond}}$) drops generally with the increase of energy as shown in Fig. 2b (the criteria of H-bonds are (i) N–H$\cdots$O distance $<$2.5 Å and (ii) angle $\angle$NHO $>$ 90°). $N_{\text{H-bond}}$ varies largely from crystal to crystal in a wide range from 2 to 6 per molecule, but reduces smoothly in an amorphous region from ~3.4 to ~2.9 per molecule.

It should be mentioned that for the six crystals in Table 1, urea molecules are in a C_{2v} point symmetry in phases **I**, **IV** and **C**,

and the symmetry breaks in other crystals, for example, it is C_s in crystal **A** and only C_1 in phase **III** and **B**. The urea molecules lie flat only in phase **I**, and are buckled in other crystal structures. The dihedral angles H–NC–H are 170° in phase **IV**, 140° and 160° in phase **III**, and 160° in crystals **A** and **C**. The H-bond distances vary from 1.96 Å to 2.37 Å in these crystals (Table 1). The typical type-I H-bonds are about 2.15 Å, appearing in phases **I**, **IV** and **A**, being longer than that of type-II and type-III. Both the shortest and the longest H-bonds appear in phase **III**, corresponding to two type-I H-bonds.

For 25 low energy crystals refined using DFT, we note that all these crystal forms obtained from Amber global PES sampling remain as stable structures (with the same symmetry) under DFT (BEEF-vdW) optimization; however, Amber predicts phase **IV** as the GM, but DFT predicts phase **III** as the GM. Experimentally, phase **I** is the observed crystal form under ambient conditions and it will turn to phase **III** at 0.48 GPa. Phase **IV** is only observed at even higher pressure, above 2.8 GPa, in experiments.[9] The energy difference between phase **I** and **III** is only 0.26 kcal mol^{-1} from DFT, but 0.42 from Amber. While it remains unclear whether the experimentally observed phase **I** is indeed the GM for a urea molecular crystal, the results from DFT (BEEF-vdW) appear to be more consistent with the existing experimental findings. We emphasize that if no vdW term is present in DFT calculations (see the ESI†), the crystal structures turn out to be unstable (such as phase **I**, being 0.86 kcal mol^{-1} less stable than crystal **A**), suggesting the importance of vdW interaction in molecular crystals. Due to the small energy difference between these crystals (within 1.5 kcal mol^{-1}), the overall consistency between Amber and DFT calculations suggests that the global PES presented here can capture the main physical picture for the urea crystal PES.

From the global PES of urea, we confirm that unlike typical covalent and metallic solids, there are many energetically nearly-degenerate crystal structures near the GM for molecular crystals as represented by urea. It is therefore interesting to ask whether the crystal-to-crystal conversion is also facile between these crystal forms. We next applied the SSW reaction pathway sampling to explore the low energy pathways linking the representative crystal structures (phase **IV** to **C**) in Table 1 to phase **III** (the GM under DFT). The detail of the pathway sampling is described in Section 2. From the lowest energy pathway between crystals, we have obtained the reaction barriers of the transitions, which are listed in Table 1 (the data with the Amber force field are also listed in Table S2 (ESI†), and are consistent with the barriers from DFT).

As a representative, we show the reaction profile connecting low energy crystals and highlight the reaction snapshots from phase **C** to **III** in Fig. 3 (those for **B** to **A** are shown in the ESI,† Fig S2). It is interesting to find that these crystal-to-crystal transition reactions can be classified into three types according to the H-bond network. (i) For the three experimentally observed phases (**I**, **III** and **IV**) sharing the same H-bond network, *i.e.* type I and II, the barriers are very low, <0.1 kcal mol^{-1}; (ii) for crystals maintaining type-I but not type-II, including **A** and **C**, the barriers increase to 0.2–0.4 kcal mol^{-1}; and (iii) for crystals (crystal **B**) lacking a type-I H-bond network, the barrier becomes much higher, being 2.24 kcal mol^{-1}. This indicates that the structural similarity, characterized by the H-bond network, is critical for the transition kinetics. Because these lowest energy minima (except crystal **B**) on the global PES are separated by a low barrier less than k_BT ($\sim$0.6 kcal mol^{-1} at 300 K), one would expect that the transition between them is kinetically rapid as driven by thermal fluctuation.

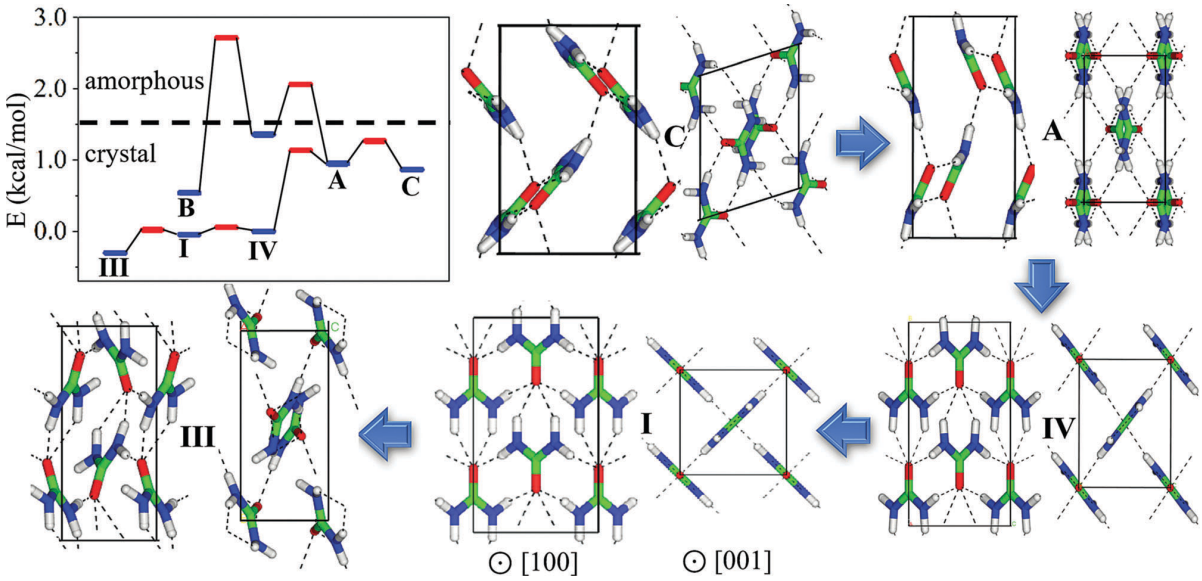

Fig. 3 Crystal-to-crystal transition energy profile and reaction snapshots in urea from DFT (BEEF-vdW). For each snapshot, two view angles, [100] and [001] with reference to crystal phase **I** lattice, are shown.

To better understand the reaction kinetics, we have analyzed the molecular displacement pattern during the crystal-to-crystal transitions, as shown in Fig. 3. The low barrier reaction, **I**-to-**IV** with the same type-I H-bond network, is achieved by the continuous compression of the lattice along the [010] direction (all directions/planes are with reference to the crystal **C** lattice) that is accompanied by the rotation of each molecule around the C_2 axis of urea. As a result, the transition leads to the decrease of the volume from 78.4 (**I**) to 76.3 (**IV**) Å^3 per molecule. It is important to notice that no H-bond breaks through the process and the OP_4 is always kept as 1.0, supporting the low barrier transition between them. Similarly, the **I**-to-**III** transformation is also a low-barrier reaction involving mainly the lattice compressing together with a low-degree of twisting of molecules. The transitions from **IV** to **A** and to **C** create the new type-III H-bond network at the expense of the weakening of the type-I network. This process features the tilting of each molecule towards the (100) plane, which effectively expands the volume of the crystal. The reaction from **A** to **C** breaks one H-bond per molecule and thus increases the barrier. Apparently, all these low barrier crystal-to-crystal transition reactions follow the diffusionless mechanism where each molecule experiences only local rotation with a minimum destruction to the H-bond network. By contrast, the pathway from crystal **B** to **A** (shown in the ESI,† Fig. S2), due to the distinct H-bond network between them, has a high barrier (2.24 kcal mol^{-1}), where 50% of the H-bonds in **A** break in the reaction.

With the kinetics data of crystal-to-crystal transition, we may summarize the global PES (zero temperature) for urea schematically in one-dimension as Fig. 4a. For urea solid, a large single funnel containing the GM (E_{gm}) is now identified from theory, where the bottom of the funnel is flat and the crystal structures inside this funnel can transform facilely from one to another. While there are less stable crystal forms ($E_{cry\text{-}h}$), they locate in other small funnels, for example, where the crystal **C** of urea sits, and their transformation to the GM crystal is hindered by a high solid-to-solid barrier. Upon the increase of temperature, due to their large entropy, the liquid-like (melt) states become dominate in the free energy surface (FES), as schematically plotted in Fig. 4b. Only the most stable crystals in the large funnels with the chemical potentials lower than that of the melts ($\mu_{cry} < \mu_{liq}$) remain in the bottom of the free energy profile, while the other less stable crystals in the small funnels smear into the high density liquid states.

By comparing the PES and FES, it can be seen that the crystal-to-crystal transition barrier is critical for the (fast) growth of large molecular crystals. A low barrier in crystal-to-crystal transition allows the rapid transformation between low energy crystal forms and they finally converge to the energetically most favoured form at the reaction conditions. For urea crystallization from melts, our results show that the crystal-to-crystal barrier ($\mu^{\neq}$ in Fig. 4b) is lower than 0.4 kcal mol^{-1}, which could be sufficiently lower than the chemical potential of melts (μ_{liq}). This would allow the crystal-to-crystal transition in combination with the crystallization of melts towards the large funnel crystals (such as phase **I**, **III** and **IV**) with a lower chemical potential (μ_{cry}). It is noticed that the other less stable crystals in the small funnel

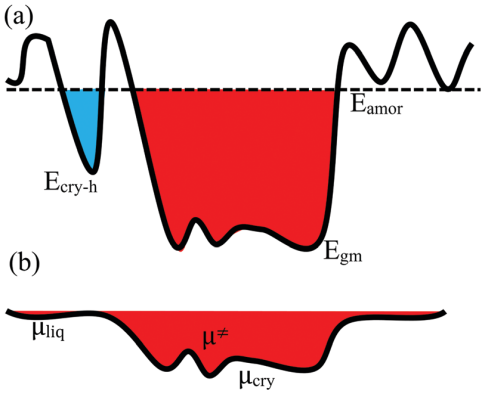

Fig. 4 Illustration of the simplified PES (a) and the free energy surface (b) of urea molecular crystals in 1-D. In the potential energy surface (a), E_{gm}, $E_{cry\text{-}h}$ and E_{amor} stand for the energy for the lowest energy crystal, for the metastable crystal separated by a high energy crystal-to-crystal barrier, and for the amorphous structures (an averaged value as indicated by the dashed black line), respectively. At finite temperatures where the free energy surface (b) matters, the chemical potential μ of melts μ_{liq} gets close to the most stable crystal forms (μ_{cry}) due to the entropy effect. Different crystal forms in the large funnel are separated by a maximum barrier height $\mu^{\neq}$, which should be lower than μ_{liq}. The high energy crystal forms with low configurational density smear into the high density liquid states at high temperatures.

are thermodynamically disfavoured (even though kinetically they may form, they will prefer to melt reversibly). Therefore, we can conclude that for a rapid crystallization from melts, two key features of the PES for molecular crystals must be present: (i) the most stable crystal structures appear in the large funnel and (ii) the transition barrier must be low enough between these stable crystals in the same large funnel to allow a fast growth of the crystal during the crystallization. Obviously, the urea crystal is special because it has a dominant type-I H-bond network, which not only stabilizes the crystals but also facilitates the transformations among them.

4. Conclusions

To conclude, with SSW global exploration, the global PES of urea crystals including both minima and pathways is now established. This allows us to pinpoint a principal H-bond network (type-I in urea) that connects to the solid-to-solid transformation kinetics of urea, although the strong effect of directional H-bonds in molecular packing has long been expected.[31] This success holds the promise of designing functional molecular crystals by predicting their properties using the computed global PES from first principles.

In particular, in addition to previously reported ones, namely phases **I**, **III** and **IV** by experiments and form II by theoretical simulations, seven new crystal phases of urea are identified that have a <1 kcal mol^{-1} energy difference with respect to the global minimum (phase **III**). In urea, the Kitaigorodskii rule is not perfectly obeyed, where the densest crystal form is not the energetically more favored due to the presence of strong

H-bonds. The crystal-to-crystal transformation barrier between phases with the same H-bond network is below 0.2 kcal mol^{-1}, while that between crystals with different H-bond networks is much higher, being 2.24 kcal mol^{-1}.

Conflicts of interest

There are no conflicts to declare.

Acknowledgements

This work was supported by the National Science Foundation of China (21603035 and 21533001), the Science and Technology Commission of Shanghai Municipality (08DZ2270500), and the Shanghai Pujiang Program (16PJ1401200).

Notes and references

1 L. Yu, *Acc. Chem. Res.*, 2010, **43**, 1257–1266.
2 G. R. Desiraju, *J. Am. Chem. Soc.*, 2013, **135**, 9952–9967.
3 S. L. Price, D. E. Braun and S. M. Reutzel-Edens, *Chem. Commun.*, 2016, **52**, 7065–7077.
4 M. K. Panda, S. Ghosh, N. Yasuda, T. Moriwaki, G. D. Mukherjee, C. M. Reddy and P. Naumov, *Nat. Chem.*, 2015, **7**, 65–72.
5 P. Naumov, S. Chizhik, M. K. Panda, N. K. Nath and E. Boldyreva, *Chem. Rev.*, 2015, **115**, 12440–12490.
6 J. Bauer, S. Spanton, R. Henry, J. Quick, W. Dziki, W. Porter and J. Morris, *Pharm. Res.*, 2001, **18**, 859–866.
7 F. Giberti, M. Salvalaglio, M. Mazzotti and M. Parrinello, *Chem. Eng. Sci.*, 2015, **121**, 51–59.
8 T. Mandal and R. G. Larson, *J. Chem. Phys.*, 2017, **146**, 134501.
9 A. Olejniczak, K. Ostrowska and A. Katrusiak, *J. Phys. Chem. C*, 2009, **113**, 15761–15767.
10 C. Shang and Z. P. Liu, *J. Chem. Theory Comput.*, 2013, **9**, 1838–1845.
11 C. Shang, X.-J. Zhang and Z.-P. Liu, *Phys. Chem. Chem. Phys.*, 2014, **16**, 17845–17856.
12 J. Wellendorff, K. T. Lundgaard, A. Møgelhøj, V. Petzold, D. D. Landis, J. K. Nørskov, T. Bligaard and K. W. Jacobsen, *Phys. Rev. B: Condens. Matter Mater. Phys.*, 2012, **85**, 235149.
13 Y.-P. Xie, X.-J. Zhang and Z.-P. Liu, *J. Am. Chem. Soc.*, 2017, **139**, 2545–2548.
14 X.-J. Zhang and Z.-P. Liu, *Phys. Chem. Chem. Phys.*, 2015, **17**, 2757–2769.
15 S. Plimpton, *J. Comput. Phys.*, 1995, **117**, 1–19.
16 V. Hornak, R. Abel, A. Okur, B. Strockbine, A. Roitberg and C. Simmerling, *Proteins: Struct., Funct., Bioinf.*, 2006, **65**, 712–725.
17 M. W. Schmidt, K. K. Baldridge, J. A. Boatz, S. T. Elbert, M. S. Gordon, J. H. Jensen, S. Koseki, N. Matsunaga, K. A. Nguyen, S. Su, T. L. Windus, M. Dupuis and J. A. Montgomery, Jr., *J. Comput. Chem.*, 1993, **14**, 1347–1363.
18 P. J. Stephens, F. J. Devlin, C. F. Chabalowski and M. J. Frisch, *J. Phys. Chem.*, 1994, **98**, 11623–11627.
19 A. D. Becke, *J. Chem. Phys.*, 1993, **98**, 5648–5652.
20 C. Lee, W. Yang and R. G. Parr, *Phys. Rev. B: Condens. Matter Mater. Phys.*, 1988, **37**, 785–789.
21 C. I. Bayly, P. Cieplak, W. D. Cornell and P. A. Kollman, *J. Phys. Chem.*, 1993, **97**, 10269–10280.
22 J. Wang, R. M. Wolf, J. W. Caldwell, P. A. Kollman and D. A. Case, *J. Comput. Chem.*, 2004, **25**, 1157–1174.
23 C. Caleman, P. J. van Maaren, M. Hong, J. S. Hub, L. T. Costa and D. van der Spoel, *J. Chem. Theory Comput.*, 2012, **8**, 61–74.
24 M. Salvalaglio, T. Vetter, M. Mazzotti and M. Parrinello, *Angew. Chem., Int. Ed.*, 2013, **52**, 13369–13372.
25 G. Kresse and J. Furthmuller, *Comput. Mater. Sci.*, 1996, **6**, 15–50.
26 G. Kresse and J. Furthmüller, *Phys. Rev. B: Condens. Matter Mater. Phys.*, 1996, **54**, 11169–11186.
27 P. E. Blöchl, *Phys. Rev. B: Condens. Matter Mater. Phys.*, 1994, **50**, 17953–17979.
28 A. I. Kitaigorodsky, *Molecular crystals and Molecules*, Academic Press, New York, 1973.
29 P. J. Steinhardt, D. R. Nelson and M. Ronchetti, *Phys. Rev. B: Condens. Matter Mater. Phys.*, 1983, **28**, 784–805.
30 X.-J. Zhang, C. Shang and Z.-P. Liu, *Phys. Chem. Chem. Phys.*, 2017, **19**, 4725–4733.
31 M. C. Etter, *Acc. Chem. Res.*, 1990, **23**, 120–126.